

A new digital pulse processing method for $2\pi\alpha$ and $2\pi\beta$ emitter measurement

Zheng Tu¹ · Ke-Zhu Song¹ · Ming Zhang² · Zhi-Jie Yang² · Zhi-Guo Ding¹ · Hong-Wei Yu¹ · Jun-Cheng Liang² · Hao-Ran Liu²

Received: 20 April 2016/Revised: 20 July 2016/Accepted: 29 July 2016/Published online: 13 October 2016
© Shanghai Institute of Applied Physics, Chinese Academy of Sciences, Chinese Nuclear Society, Science Press China and Springer Science+Business Media Singapore 2016

Abstract Digital pulse processing has developed rapidly during recent years. Moreover, it has been widely applied in many fields. In this study, we introduce a digital pulse processing method for $2\pi\alpha$ and $2\pi\beta$ emitter measurement. Our digital pulse processing method for $2\pi\alpha$ and $2\pi\beta$ emitter measurement is comprised of a field-programmable gate-array-based acquisition card and a pulse-height analysis routine. We established two channels (one for the α emitter and one for the β emitter) on an acquisition board using an analog-to-digital converter with a 16-bit resolution at a speed of 100 million samples per second. In this study, we used captured and stored data to analyze emission rate counts and spectrums. The method we established takes into account noise cancelation, dead-time correction, background subtraction, and zero-energy extrapolation. We carefully designed control procedures in order to simplify pulse-width fitting and threshold-level setting. We transmitted data and commands through a universal serial bus between the acquisition board and the computer. The results of our tests prove that our method performs well in pulse reconstruction fidelity and amplitude measurement accuracy. Compared with the current standard method for measuring $2\pi\alpha$ and $2\pi\beta$ emission rates, our system demonstrates excellent precision in emission rate counting.

Keywords Digital pulse processing · α and β emitter measurement · FPGA

1 Introduction

Digital pulse processing is a signal processing technique in which detector signals (preamplifier or shaping amplifier output) are digitized and processed in order to extract information. Such techniques have undergone rapid development in recent decades [1–3]. These new techniques have been applied in many fields [4–6]. The main advantages of digital pulse processing (compared to analog-based processing) have been summarized in previous studies [7]. In this study, we developed a custom-built digital pulse processing method comprised of a field-programmable gate-array (FPGA)-based acquisition card with a 16-bit resolution at a sampling rate of 100 million samples per second (MSPS). Moreover, we developed a method to analyze pulse height in order to determine the surface emission rate measurements for α and β emitters.

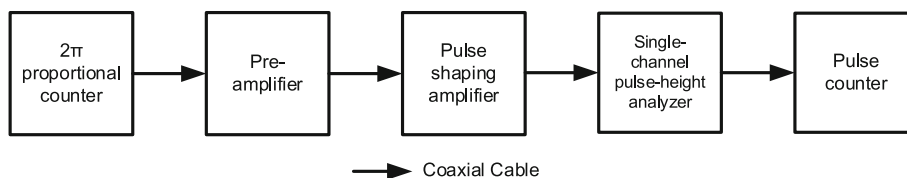
The main objective of this study was to develop a digital pulse processing method to replace the current instrumentation-based $2\pi\alpha$ and $2\pi\beta$ emitter measurement system [8]. The instrumentation-based system serves as a national primary standard at the National Institute of Metrology (NIM) and ensures the traceability of α and β surface emission rates. A basic block diagram of the standard analog emitter measurement system is shown in Fig. 1. In the standard analog system, the detected α or β signal is processed through the preamplifier, the pulse-shaping amplifier, and the single-channel pulse-height analyzer (SCA), successively [9–12]. The pulse counter records signals when there are pulses generated from the SCA. The

✉ Ke-Zhu Song
skz@ustc.edu.cn

¹ State Key Laboratory of Particle Detection and Electronics, University of Science and Technology of China, Hefei 230026, China

² National Institute of Metrology, 18 North Third Ring East Rd., Beijing 100029, China

Fig. 1 Simplified block diagram of the standard analog emitter measurement system



amplitude of the analog pulse at the output of the pulse-shaping amplifier is typically proportional to the energy of the detected event of the particle. Selection of a range of signal levels at the output of the amplifier is equivalent to the selection of a range of energies for these events [13]. The SCA accomplishes the selection by producing an output logic pulse for the pulse counter when the amplitude of an input signal falls within the pulse-height window established by two preset threshold levels. In our method, signal acquisition and analysis determine the functions of the SCA and pulse counter.

The advantages of utilizing a digital pulse processing system are as follows: First, signal capture and processing allow for offline analysis and corrections, including noise cancelation, dead-time correction, and background subtraction. Second, control procedures provide flexible options for pulse-width fitting and threshold-level setting (as determined by the needs of the surveyor). Third, energy extrapolation can be conducted to correct for β counting loss due to the continuous β energy spectrum. By manipulating the selected pulse, one can change the threshold for β counting in the data and thus avoid statistical uncertainty from repetitive measurements. Furthermore, digitized pulse processing allows for further operations, such as shape discrimination for different particles.

2 Structures of the system

Our digital pulse processing method consists of an acquisition board and a computer running the control and analysis program, as shown in Fig. 2. The acquisition board captures and digitalizes the pulse and then selects the height of the pulse before transferring it to the computer. We used universal serial bus (USB) protocols for transmission, specifically a USB protocol with a micro-USB peripheral controller on board called CYPRESS CY7C68013A [14].

In order to meet the different requirements for the acquisition of α and β emitter signals, we utilized separate conditioning amplifiers, in the front of the input side, to ensure the range of signal amplitudes was suitable for the range of the analog-to-digital converter (ADC) inputs [15]. According to the tests completed using the oscilloscope (Agilent Technologies MSO6034A), the α signal from the pulse-shaping amplifier (ORTEC 572A) had an amplitude

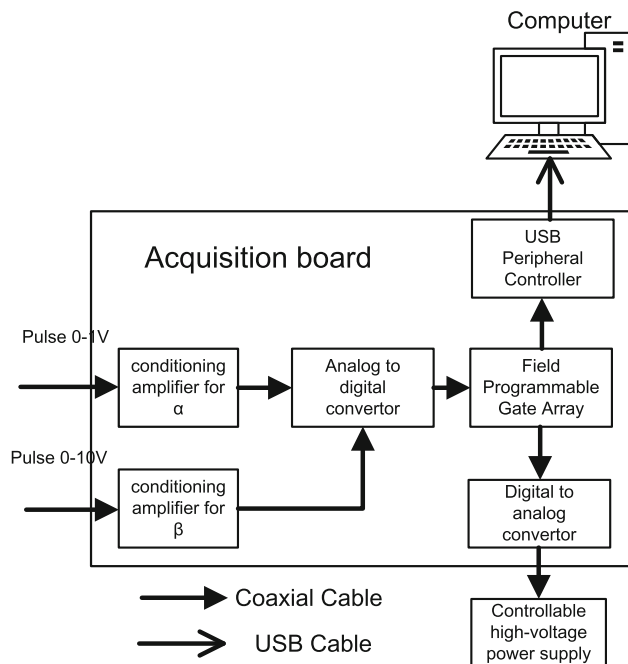


Fig. 2 Simplified block diagram of the digital pulse processing system

range of 0–1 V, and the β signal had an amplitude range from 0 to 10 V. Both signals were single ended from the pulse-shaping amplifier with a 50- Ω characteristic impedance coaxial cable. To create a differential ADC with an input range from -1 to 1 V, we chose TI LMH6554 (a conditioning amplifier chip) because of its exceptional signal fidelity and wide large-signal bandwidth (which is necessary for 8- to 16-bit high-speed data acquisition systems) [16, 17].

In order to acquire both α and β signals, we used an ADC with two channels of 16 bits and 100 MSPS. According to ISO 8769, for the emission rate measurement of the β source, the measurement threshold should be 590 eV, which is equal to 10 % of the energy of the ^{55}Fe X-ray. So the voltage should be 20 mV at 1600-V high-voltage supply on the basis of experimental measurements. As the signal pulse has 10 V margin (maximum), the minimum voltage was chosen to be 2.5 mV to increase the precision as much as possible and to determine the emission rate measurement of the β source. Moreover, 100 MSPS is sufficient for sampling because the width of the signal, which is able to trigger the amplitude discriminator, needs to be less than 100 ns. As a result, we chose ADI AD9268 (a standard ADC chip) for the acquisition

process. According to the completed tests, the signal-to-noise ratio (SNR) of AD9268 at 100 MHz was 74.3 dB (Signal generator: Tektronix AWG5000 series: 600 MS/s maximum sampling rate, 2.5 G bandwidth, 14-bit D/A resolution, 16 M memory length). While it was lower than the 78.2 dB shown in the datasheet of the device [18], it still meets the requirement of the minimum voltage precision.

In this study, we used a digital-to-analog convertor (DAC) and a controllable high-voltage power supply to achieve high-voltage control. The DAC provided a control voltage of 0–5 V (as determined by the configuration set by the user on the computer). The high-voltage power supply transformed 15 V DC input into 0–3 kV output voltages, varying linearly with the control voltage. We chose TI DAC8881 (a DAC chip) for our method because of its linearity and low-power operation [19].

3 FPGA logic module

The schematic diagram of the FPGA is shown in Fig. 3. As there is a 16-bit channel for both the α data and the β data in the AD9268, the interface for the ADC is a 32-bit complementary metal–oxide–semiconductor (CMOS) with a clock of 100 MHz. We utilized the ALTERA Cyclone V in order to guarantee that the FPGA would work well and have sufficient memory blocks [20]. The data sampled by the ADC were screened in the amplitude discriminator. When the input signal exceeded a preset acquiring threshold level, the amplitude discriminator generated a trigger signal. This threshold level was set below that of the traditional SCA in order to acquire more pulse signals for analysis. To reduce the effects of the high-frequency noise, we established a hold time in order to ensure the over-threshold state was not instantaneous. After the over-threshold was detected, we introduced a fixed dead time in

order to prevent any other over-threshold detections. This helped us discard the tails of pulses with long time widths and the small pulses after a main pulse (an occurrence known as the ringing effect).

Signals were entered into the data buffer, in the form of data packages, when all the requirements were met. The data package, as listed in Table 1, had 128-byte data for each selected signal pulse. Each data package had 60 sample points. At the sample rate of 100 MHz, we obtained a sample point every 10 ns. As such, in order to record a pulse with a time width of about 10 μ s in just one package, a mid-value point was extracted from every 16-sample points. This process sacrificed some of the utilization rate of the sampling, but it was necessary for analysis. For pulses with different time widths, the extraction ratio can be adjusted through configuration.

All the data collected in the data buffer were transferred to the USB peripheral controller at a speed of 48 million bytes per second (MBPS). According to the tests we conducted, the speed of the transmission between the USB peripheral controller and the computer was 11.2 MBPS. When there were 20,000 pulses per second, 5.12 Mbytes of data were transferred ($20,000 \times 2 \times 128$ byte). Our tests show that our method works very well at this pulse rate (and meets the requirements for most emitter measurements).

The surveyor controlling the system can conveniently set the parameter configuration of the amplitude discriminator and high-voltage controller by transferring the command to the FPGA through the USB peripheral controller. As there is a time margin in data transmission, occupation of the USB data bus has no influence on our method’s operations (which we proved conclusively in our tests).

4 Control and analysis programs

The analysis program contains an online mode and an offline mode. The flow diagram of the analysis program is shown in Fig. 4. In the online mode, before the acquisition, the surveyor must set the parameters of the amplitude discriminator in the FPGA (the parameters being the acquiring threshold level, hold time, acquisition time, and the extraction ratio). Each configuration command is also sent as a command package, as listed in Table 2.

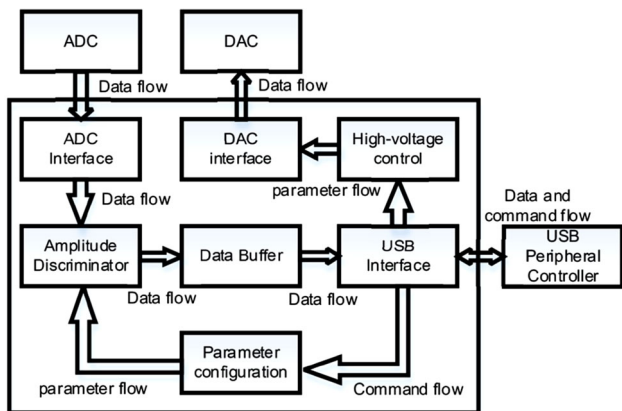


Fig. 3 Schematic diagram of the FPGA

Table 1 Form of the data package used in the pulse processing system

Data package (128 bytes)			
Package head	Event counts	Time stamp	Content
(2 bytes)	(2 bytes)	(4 bytes)	(120 bytes)

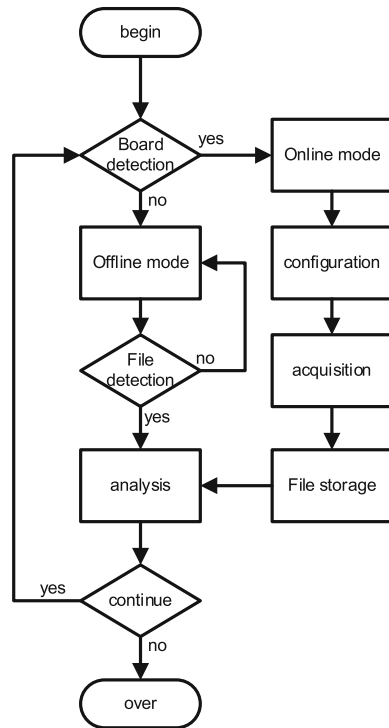


Fig. 4 Flow diagram of the control and analysis program

The received data are stored in the computer as a hex file (in the form of a data package). For convenience sake, the data are stored in one file every minute in sequence. The pulse-shape analysis process automatically reads the file regardless of whether it is in online mode or offline mode. In the analysis, the pulse amplitude was extracted from the data and then compared with threshold. The threshold level can be set according to the demands of the surveyors. Thus, the pulse counts in the range of the preset threshold are easily calculated out. Besides the amplitude analysis, the width of the pulse is also taken into account in order to exclude the ambient noise. Full width at half maximum (FWHM) is calculated for every pulse. The signal with a FWHM in a certain range is regarded as the signal pulse, and the other pulses are treated as ambient noise pulses [21].

By utilizing the procedures outlined above, the counts of the α and β pulses (at specific threshold levels) provide conclusive results. According to the spectrum of the α source, the energy of the pulses is concentrated near its

spectral line. Therefore, we only need to set an appropriate threshold level and make the necessary calculations in order to determine the event counts for the α emitter. However, for the β emitters, according to the spectrum of the $^{90}\text{Sr}/^{90}\text{Y}$, the energy of the pulses is distributed over the entire spectrum. As such, we need to extrapolate in order to obtain the zero-energy counting rates. The spectrum of the β sources can be obtained by setting threshold levels according to the results of each signal measurement. The counting rates of the different threshold levels can then be used to determine the linear fitting, which, in turn, yields the counting rate of the β source. Importantly, the dead time during the acquirement of the signal should be counted in order to correct the counting rate [22]. The corrected counting rate is

$$N' = \frac{N}{1 - \tau * N}$$

where N is the counting rate (s^{-1}) of measurement, and τ is the dead time (μs) of the acquisition (which can be set by the surveyors).

5 System validation

In order to test our method’s ability to reconstruct pulses, we first used a signal generator (Tektronix AFG3251 series) to simulate the pulses generated by the α and β sources. Both of the α and β pulses from the pulse-shaping amplifier were Gaussian-like pulses. We used a $50\text{-}\Omega$ resistance channel to simulate the pulses and fanned them out by the connector. We sampled the signals with an oscilloscope (Tektronix MSO5204) and our method simultaneously. The α pulse had a $2.4\text{-}\mu\text{s}$ FWHM with an amplitude of 200 mV , as shown in Fig. 5a. The β pulse had a $2.4\text{-}\mu\text{s}$ FWHM with an amplitude of 5 V , as shown in Fig. 5c. The pulses were triggered by a random external trigger source at a 20 K/s triggering rate. The results of the test demonstrate that our method works very well. The sampled pulses were reconstructed in order to compare them with the pulses sampled by the oscilloscope. The restored α pulse sampled by our method is shown in Fig. 5b. The reconstructed β pulse sampled by our method is shown in Fig. 5d. Compared with the measurements from the oscilloscope, we found that our method recreated the shape of the pulse with high fidelity. This level of accuracy is crucial for pulse-shape analysis.

In order to verify the accuracy of the acquisition channels, we used a signal generator to generate sine waves for amplitude tests. The sine waves had a $20\text{-}\mu\text{s}$ period and various peak-to-peak values. After capturing and digitalizing the sine waves, the peak-to-peak values (V_{pp}) of the reconstructed waves were measured and compared with

Table 2 Form of the command package used in the pulse processing system

Data package (10 bytes)			
Package head	Command number	Parameter	Package tail
(2 bytes)	(2 bytes)	(4 bytes)	(2 bytes)

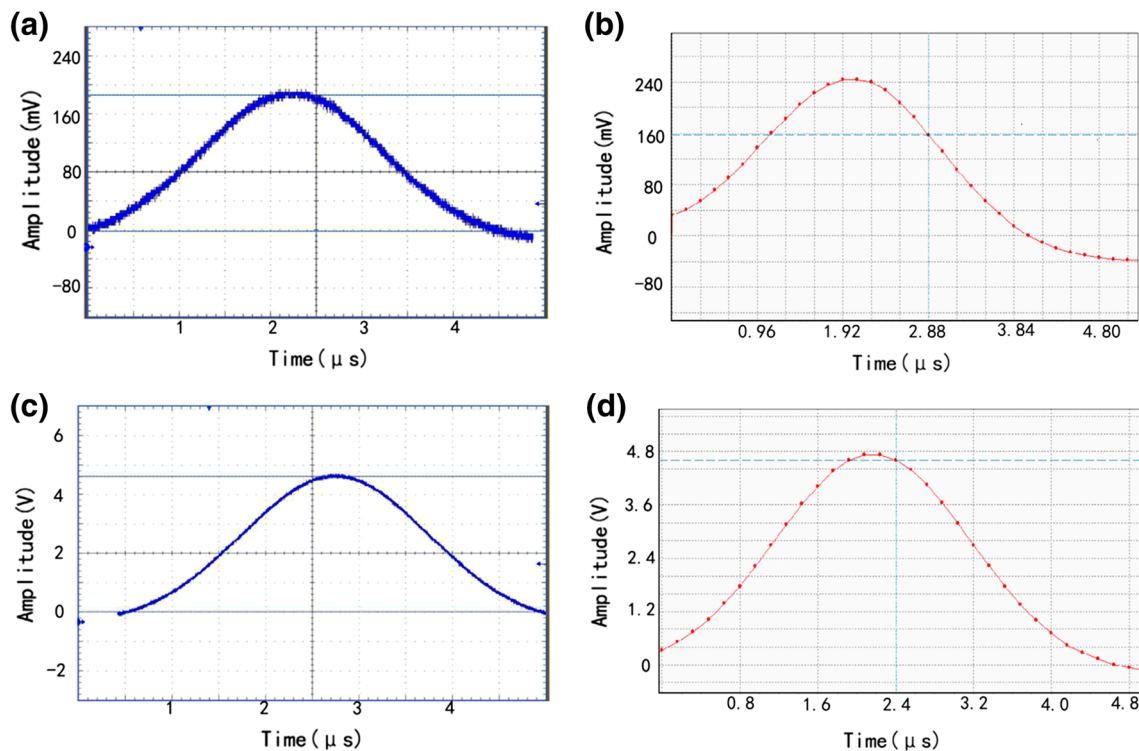


Fig. 5 **a** Simulated α pulse sampled by the oscilloscope; **b** reconstructed α pulse sampled by our method; **c** simulated β pulse sampled by the oscilloscope; **d** reconstructed β pulse sampled by our method

those it had generated. The results of the amplitude tests of the α channel are listed in Table 3. The results of the amplitude tests of the β channel are listed in Table 4. We found minor errors in both channels, which were all below 1 % and sufficient for processing.

Table 3 Comparison of the peak-to-peak values between generated waves and restored waves, as sampled by the α channel of our pulse processing method

V _{pp} of generated waves (mV)	V _{pp} of reconstructed waves (mV)	Difference (mV)	Percent of difference
50	50.408	0.408	0.816
60	60.510	0.510	0.850
70	70.306	0.306	0.437
80	80.204	0.204	0.255
90	90.204	0.204	0.227
100	100.714	0.714	0.714
150	148.877	-1.122	-0.748
200	198.775	-1.224	-0.612
300	299.489	-0.510	-0.170
400	397.857	-2.142	-0.536
500	498.265	-1.734	-0.347
600	598.061	-1.938	-0.323
800	796.122	-3.877	-0.485

We conducted the spectrum measurement in the National Metrology Institute of China, using the newly designed multi-wire proportional counter. The sources used for measurement were the α emitters (Pu-239 and Am-241) and the β emitters (Sy-90/Y-90). The emitters were incorporated into the surface of an anodized aluminum foil approximately 0.3 mm thick. The anodized aluminum foil was then placed in the center position of the detecting area. The measurements were taken at 0.1 MPa with 100 mL/min gas flow speed with a mixture of 90 % argon gas and 10 % methane by volume. The preamplifier was a CAN-BERRA MODEL 2006, and the pulse-shaping amplifier was an ORTEC 572A. The voltages were set as 700 V for the α emitters and 1600 V for the β emitters. The spectrum for the α emitter Pu-241 obtained by using our method is shown in Fig. 6. The spectrum for the β emitter Sy-90/Y-90 obtained by using our method is shown in Fig. 7.

We conducted a counting rate measurement under the conditions of the spectrum measurements outlined above. As there were two output channels on the pulse-shaping amplifier ORTEC 572A, we were able to simultaneously conduct measurements using both methods (one channel using our method and the other channel using SCA and the pulse counter). The acquiring threshold of our method was set to 40 mV for the α channel and 10 mV for the β channel. The threshold of SCA was set to 60 mV for the α source and 20 mV for the β source. Analysis processes of

Table 4 Comparison of the peak-to-peak values between generated waves and reconstructed waves, as sampled by the β channel of the pulse processing method

Vpp of generated wave (mV)	Vpp of acquired wave (mV)	Difference (mV)	Percent of difference
50	49.668	-0.331	-0.662
100	99.337	-0.662	-0.662
200	201.986	1.986	0.993
300	298.675	-1.324	-0.442
400	401.986	1.986	0.497
500	500.000	0	0.000
600	604.635	4.635	0.773
800	800.000	0	0.000
1000	1002.649	2.649	0.265
2000	2005.960	5.960	0.298
3000	2999.337	-0.662	-0.022
4000	3980.794	-19.205	-0.480
5000	4956.953	-43.046	-0.861

our method set the threshold value equal to that of SCA. The dead time of our method was set to 10 μ s, and the hold time was set to 100 ns.

According to the measurement results, the counts measured by our method were greater than that displayed by the pulse counter. This result reflects the more precise identifiable pulse width in our method than of that in SCA. In order to reduce the effects of ambient noise, we conducted measurements at a working voltage of 1600 V (without emitters in the detector). The mean value of the ambient counting rates was 34.911 for our method and 30.988 for the ORTEC SCA.

For the sake of correctness, we conducted additional measurements with different set dead times in order to

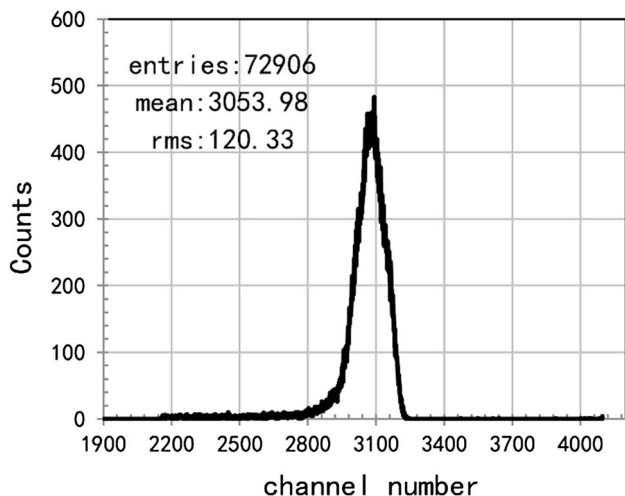


Fig. 6 Spectrum of the α emitter Am-241 obtained by using our pulse processing method

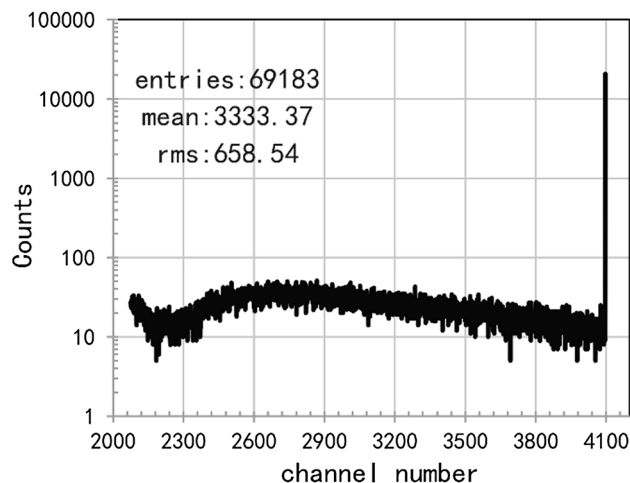


Fig. 7 Spectrum of the β emitter Sr-90/Y-90 obtained by using our pulse processing method

Table 5 Results of the counting rate and the fixed counting rate with different set dead times using a 90Sr/90Y emitter

Emitter	Dead time (μ s)	Counting rate (s^{-1})	Fixed counting rate (s^{-1})
90Sr/90-2Y	10	231.54	232.08
	15	230.51	231.32
	30	229.54	231.15
	60	228.46	231.66
	80	226.48	230.72

verify the algorithm of our dead-time correction. As listed in Table 5, we used the same source 90Sr/90Y with activity at magnitude of 10^2 for all measurements. In spite of the measurement errors, the results indicated that our dead-time correction was accurate and effective.

Factoring in the dead-time corrections and ambient noise subtraction, we conducted measurements for each of the six sources in order to compare our method with the ORTEC SCA and pulse counter. The uncertainty of the measurements was 0.397 and 0.885 % for the α and β channels, respectively. The results are listed in Table 6. We found that for the α channel, the percent difference between our method and the current primary standard was below 0.3 %. The percent difference for the β channel was below 1 %. These results demonstrate that our method is as accurate and precise in the measurement of the $2\pi\alpha$ and $2\pi\beta$ emission rate measurement as the primary standard method.

6 Conclusion

In this study, we presented a pulse processing method for $2\pi\alpha$ and $2\pi\beta$ emission rate measurement. Test results indicate that our method is precise in pulse reconstruction

Table 6 Comparison of the counting rates between the primary standard method and our pulse processing method

Emitter	Measurement time (min)	Counting rate of primary standard (s^{-1})	Counting rate of pulse processing system (s^{-1})	Percent of difference
239Pu	1	1718.755	1717.865	0.052
241–1Am	10	105.672	105.885	0.202
241–2Am	10	121.560	121.751	0.157
90Sr/90–1Y	10	36.288	36.013	–0.755
90Sr/90–2Y	5	194.025	195.923	0.979
90Sr/90–3Y	1	5248.218	5241.457	–0.129

and acquisition accuracy. Moreover, our method works well in obtaining spectrums because it is in good agreement with the counting rate measurement of the primary standard method used at the NIM. Furthermore, our new method is more convenient than the present method because it is operated solely by computer, which allows the digitized data to be quickly and easily analyzed. Importantly, our method is applicable to most $2\pi\alpha$ and $2\pi\beta$ emitter measurements. We will conduct further research into automatically identifying the α and β sources by analyzing the shape of the acquired pulses. We will also conduct further research into the analysis of multiple particle resources.

References

1. A. Pullia, G. Gritti, G. Ripamonti, Design of high performance digital baseline restorers. *IEEE Trans. Nucl. Sci.* **44**(3), 331–337 (1997). doi:[10.1109/23.603665](https://doi.org/10.1109/23.603665)
2. V.T. Jordanov, Real time digital pulse shaper with variable weighting function. *Nucl. Instrum. Methods A* **505**(1–2), 347–351 (2003). doi:[10.1016/S0168-9002\(03\)01094-5](https://doi.org/10.1016/S0168-9002(03)01094-5)
3. H.Q. Zhang, L.Q. Ge, B. Tang et al., Optimal choice of trapezoidal shaping parameters in digital nuclear spectrometer system. *Nucl. Sci. Tech.* **6**, 109–114 (2013). doi:[10.13538/j.1001-8042/nst.2013.06.011](https://doi.org/10.13538/j.1001-8042/nst.2013.06.011)
4. R. Grzywacz, Applications of digital pulse processing in nuclear spectroscopy. *Nucl. Instrum. Methods* **204**(1), 649–659 (2003). doi:[10.1016/S0168-583X\(02\)02146-8](https://doi.org/10.1016/S0168-583X(02)02146-8)
5. P.L. Reeder, A.J. Peurrung, R.R. Hansen et al., Detection of fast neutrons in a plastic scintillator using digital pulse processing to reject gammas. *Nucl. Instrum. Methods A* **422**(1–3), 84–88 (1999). doi:[10.1016/S0168-9002\(98\)01068-7](https://doi.org/10.1016/S0168-9002(98)01068-7)
6. R. de la Fuente, B. de Celis, V. del Canto et al., Low level radioactivity measurements with phoswich detectors using coincident techniques and digital pulse processing analysis. *J. Environ. Radioact.* **99**(10), 1553–1557 (2008). doi:[10.1016/j.jenvrad.2007.12.008](https://doi.org/10.1016/j.jenvrad.2007.12.008)
7. W.K. Warburton, M. Momayezi, B. Hubbard-Nelson et al., Digital pulse processing: new possibilities in nuclear spectroscopy. *Appl. Radiat. Isot.* **53**(4–5), 913–920 (2000). doi:[10.1016/S0969-8043\(00\)00247-5](https://doi.org/10.1016/S0969-8043(00)00247-5)
8. J.C. Liang, Q. Li, J.C. Liu et al., The absolute measurement for $2\pi\alpha$ and $2\pi\beta$ particle emission rate. *Acta Metrol. Sin.* **37**(2), 1–5 (2016). doi:[10.3969/j.issn.1000-1158.2016.00.00](https://doi.org/10.3969/j.issn.1000-1158.2016.00.00)
9. J.L. Wu, M.C. Yuan, S.H. Su et al., The alpha and beta emitter measurement system in INER. *Appl. Radiat. Isot.* **56**, 261–264 (2002). doi:[10.1016/S0969-8043\(01\)00197-X](https://doi.org/10.1016/S0969-8043(01)00197-X)
10. L.E. King, J.M.R. Hutchinson, M.P. Unterweger, A new large-area 2π proportional counting system at NIST. *Appl. Radiat. Isot.* **66**, 877–880 (2008). doi:[10.1016/j.apradiso.2008.02.079](https://doi.org/10.1016/j.apradiso.2008.02.079)
11. J.M.R. Hutchinson, S.J. Bright, The NBS large-area alpha-particle counting system. *J. Res. NBS* **92**(5), 311 (1987). doi:[10.6028/jres.092.031](https://doi.org/10.6028/jres.092.031)
12. J.C. Mostert, A primary standard for the measurement of alpha and beta particle surface emission rate at the National Metrology Institute of South Africa. *Appl. Radiat. Isot.* (2008). doi:[10.1016/j.apradiso.2008.02.059](https://doi.org/10.1016/j.apradiso.2008.02.059)
13. J.J. Wang, *Nuclear Electronics*, vol. 2 (Atomic Energy Press, Beijing, 1983), pp. 1–17. (in Chinese)
14. Y.S. Dai, L.K. Dong, Z.X. Sun et al., Design of parallel port turn USB port data acquisition system based on CY7C68013A. *Electron. Des. Eng.* **19**(16), 42–44 (2011). doi:[10.14022/j.cnki.dzsjgc.2011.16.046](https://doi.org/10.14022/j.cnki.dzsjgc.2011.16.046)
15. J.F. Chen, K.Z. Song, J.C. Liang, Dedicated $4\pi\beta$ (LS)- γ (HPGe) digital coincidence system based on synchronous high-speed multichannel data acquisition. [arXiv:1506.06008v1](https://arxiv.org/abs/1506.06008v1)
16. Q. Bichon, Optimizing the LMH6554 to drive high speed ADCs. <http://www.tij.co.jp/jp/lit/ug/tidu172/tidu172.pdf>
17. Texas Instruments. LMH6554 2.8 GHz ultra linear fully differential amplifier. <http://www.ti.com/lit/ds/sn0sb30p/sn0sb30p.pdf>
18. Analog Devices. 16-Bit, 80 MSPS/105 MSPS/125 MSPS, 1.8 V dual analog-to-digital converter (ADC). <http://www.analog.com/media/en/technical-documentation/data-sheets/AD9268.pdf>
19. Texas Instruments. 16-Bit, single-channel, low-noise, voltage-output digital-to-analog converter. <http://www.ti.com/lit/ds/sym-link/dac8881.pdf>
20. Altera Corporation. Cyclone V Device Datasheet. https://www.altera.com/en_US/pdfs/literature/hb/cyclone-v/cv_51002.pdf
21. S.R. Campbell, G.C. Stone, H.G. Sedding, Application of pulse width analysis to partial discharge detection, in *Conference Record of the 1992 IEEE International Symposium on Electrical Insulation (ISEI)*, Baltimore, MD, 07 Jun 1992, 345–348. doi:[10.1109/ELINSL.1992.246979](https://doi.org/10.1109/ELINSL.1992.246979)
22. Z.H. Wu, *Experimental Method of Nuclear Physics* (Atomic Energy Press, Beijing, 1997), pp. 22–25